https://doi.org/10.15407/ufm.27.02.175

F. MOLLAAMIN* and M. MONAJJEMI**
Kastamonu University, 37150 Kastamonu, Turkey
* fmollaamin@kastamonu.edu.tr, ** mmonajjemi@kastamonu.edu.tr

NANOENCAPSULATION OF TRANSITION METALS BY BORON NITRIDE-BASED HYBRID MATERIAL: FUTURE TRENDS OF HYDROGEN ADSORPTION TOWARDS ENERGY STORAGE

We investigate the hydrogen storage increase through doping of Cr, Ni, Zn, Mo, Pd, and Cd on the boron nitride (BN) nanocage. Based on the nuclear quadrupole resonance (NQR) analysis, Ni and Pd with atomic charges of 0.2658 and 0.3266 C on the complexes of Ni@BN and Pd@BN, respectively, have shown a much greater tendency for H_2 adsorption than other complexes. The results of nuclear magnetic resonance (NMR) spectroscopy have exhibited that the efficiency of electron admitting for implanting atoms on the [Cr, Ni, Zn, Mo, Pd, Cd]@BN through H_2 adsorption can be ordered as Ni > Pd >> Cr > Mo ≈ Zn > Cd. Regarding thermodynamic properties, for hydrogen sites in H_2 molecules, the consistencies of heteroclusters of decorated elements of Cr, Ni, Zn, Mo, Pd, and Cd can be brought up as Ni@BN > Pd@BN >> Cr@BN > Mo@BN ≈ ≈ Zn@BN > Cd@BN complexes. In addition, the hydrogen adsorption on transition metals doping BN heterocluster has been estimated through analysis of total density of states (TDOS), partial density of states (PDOS), overlap partial density of states (OPDOS) and localised orbital locator analysis (LOL). We claim that the transition metal-implanted BN can be used for designing novel materials for H_2 adsorption and sensing applications.

Keywords: hydrogen storage, boron nitride nanocage, doping, DFT

Citation: F. Mollaamin and M. Monajjemi, Nanoencapsulation of Transition Metals by Boron Nitride-Based Hybrid Material: Future Trends of Hydrogen Adsorption towards Energy Storage, *Progress in Physics of Metals*, **27**, No. 2: 175–193 (2026)

1. Introduction

Recently, doping of transition metals containing scandium, titanium, vanadium, chromium, manganese, cobalt, nickel, copper, and zinc with boron nitride nanocages has been investigated as a new method to augment the nonlinear optical (NLO) characteristics and electronic attributes [1–5].

Furthermore, hydrogen/formaldehyde adsorption on the bare boron nitride nanostructure and decorating with transition metals containing V, Cr, Mn, Nb, Mo, Tc, Ta, W, Re has been studied. The reports illustrated that the bare boron nitride shows a feeble interaction with hydrogen/formaldehyde molecules. The hydrogen/formaldehyde molecules may be forcefully adsorbed on the boron nitride doped with transition metals by considerable adsorption energy through the geometrical alteration in the transition metal doping region [6–10].

Boron nitride doped with the transition metal presents strong material candidature for flexible magnetic memory chips that are functional even under fire. Besides, spin-polarised density functional theory band structure calculations can approve clear spin asymmetry due to doping [11–16].

Due to the clear reasons mentioned above, we have explored the possibility of using boron nitride nanocages doped with Cr, Ni, Zn, Mo, Pd, Cd for H_2 saving using theoretical computations [17–19]. The structural/electronic attributes of (Cr, Ni, Zn, Mo, Pd, Cd)@BN nanocages have been evaluated using state-of-the-art computational techniques [20, 21].

Two-dimensional (2D) semiconductors have attracted considerable attention for their potential in extending Moore's law and advancing next-generation electronic devices. In this study, we have designed novel boron nitride analogues and investigated their stability and electronic properties. Furthermore, the incorporation of transition metals of Cr, Ni, Zn, Mo, Pd, and Cd at hollow sites in these analogues was explored, revealing their potential as promising electrocatalysts for hydrogen adsorption. The inclusion of transition metals significantly enhances their structural stability and electronic properties.

In this work, we reported a systematic theoretical investigation of the structural, electronic and magnetic properties of transition metal (TM) doped boron nitride. We have investigated the structural stability of the BN monolayer due to TM–TM pair co-doping and describe their interesting magneto-electronic properties as evident from the spin-polarised projected density of states. Although pristine BN is a nonmagnetic insulator, our investigation shows that the addition of a transition metal pair induced an interesting magnetic ground state. The interaction of selective TM atom pairs transferred the BN from a spin-non-polarised to a spin-polarised half-metal and semiconductor, demonstrating an effective strategy to tune the magneto-electronic properties of BN.

2. Theoretical Background, Compounds and Approaches

The goal of this investigation is to adsorb H_2 molecules by using (Cr, Ni, Zn, Mo, Pd, Cd)-implanted BN (Fig. 1) [22–26]. BN nanocage was decorated with chromium, nickel, zinc, molybdenum, palladium, and cadmium, which can augment the hydrogen adsorption potential of the BN nanocage. In our research, the calculations have been done by CAM–B3LYP–D3/

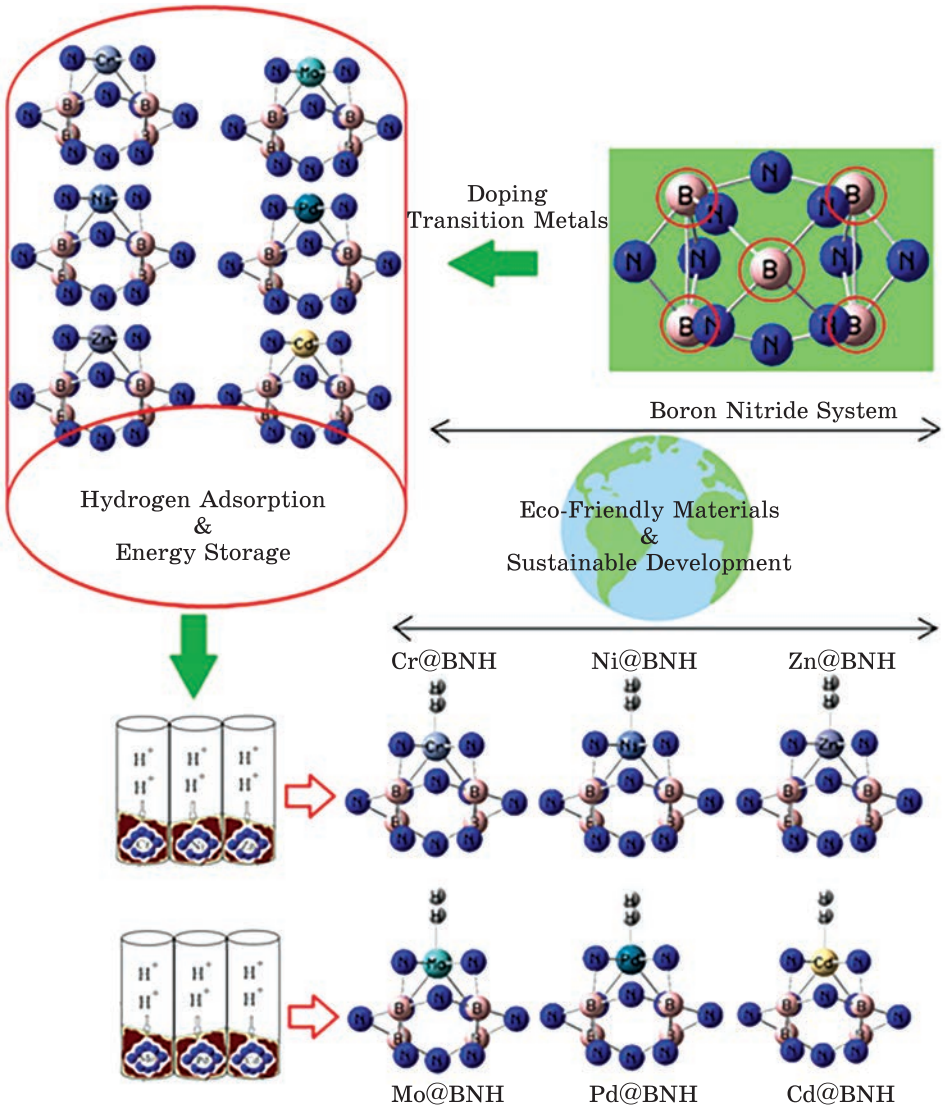

Fig. 1. Application of [Cr, Ni, Zn, Mo, Pd, Cd]@BN for adsorption of H_2 molecules in the saving energy accompanying production of Cr@BNH, Ni@BNH, Zn@BNH, Mo@BNH, Pd@BNH, and Cd@BNH heteroclusters

EPR–3, LANL2DZ level of theory. Theoretical calculations have become essential tools for a comprehensive understanding of the microscopic mechanisms in energy storage materials, particularly in charge density variations and electron transport characteristics in electrode materials. In our research, the calculations have been done at the CAM–B3LYP–D3 level of theory. A new hybrid exchange–correlation functional named the Coulomb-attenuating method (Becke, 3-parameter, Lee–Yang–Parr) (CAM-B3LYP) is proposed. It combines the hybrid qualities of B3LYP and the long-range correction. Dispersion forces were considered under the DFT-D3 method of Grimme with Becke–Johnson damping [27]. Calculations with spin polarisation were performed within the density functional theory (DFT). The exchange correlation potentials were treated using the Perdew–Burke–Ernzerhof (PBE) parameterisation within the general gradient approximation (GGA) [28–30].

Figure 1 has illustrated the status adsorption of H_2 molecules on the [Cr, Ni, Zn, Mo, Pd, Cd]@BN surface, which leads to the formation of complexes containing Cr@BNH, Ni@BNH, Zn@BNH, Mo@BNH, Pd@BNH, and Cd@BNH.

The charge distribution of the mentioned complexes is calculated using the Bader charge analysis [31–34]. The trapping of H_2 molecules by [Cr, Ni, Zn, Mo, Pd, Cd]@BN was successfully incorporated due to binding formation consisting of Cr@BNH, Ni@BNH, Zn@BNH, Mo@BNH, Pd@BNH, and Cd@BNH (Figure 1).

In this article, the rigid potential energy surface (PES) using DFT [35–38] calculations has been computed using Gaussian 16 revision C.01 software [39]. The input Z-matrix for adsorption of H_2 molecules by the [Cr, Ni, Zn, Mo, Pd, Cd]@BN has been designed with GaussView 6.1 [40] using 6-311 + G (d,p), EPR–3, LANL2DZ basis set [41–45].

3. Results and Discussion

3.1. TDOS/PDOS/OPDOS and Electronic Evaluation

In an isolated system (such as a molecule), the energy levels are discrete, and the concept of 'density of states (DOS)' is supposed to be completely valueless in this situation. Therefore, the 'original total DOS (TDOS)' of an isolated system can be written as [46]

$$\mathrm{TODS}(E) = \sum_i \delta(E - \epsilon_i). \tag{1}$$

The normalised Gaussian function is defined as

$$G(x) = \frac{1}{c\sqrt{2\pi}} e^{\frac{x^2}{2c^2}}, \quad c = \frac{\mathrm{FWHM}}{2\sqrt{2\ln x}}; \tag{2}$$

FWHM (full width at half maximum) is an adjustable parameter in Multiwfn [47, 48]. Furthermore, the curve map of broadened partial DOS

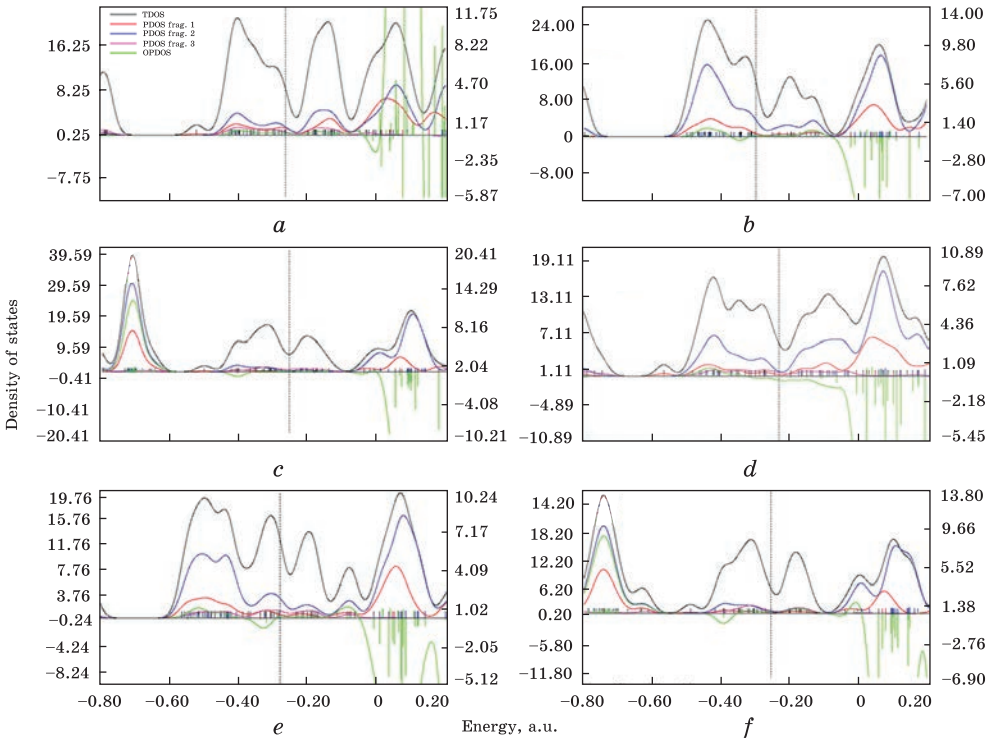

Fig. 2. TDOS/PDOD/OPDOS graphs for (*a*) Cr@BNH, (*b*) Ni@BNH, (*c*) Zn@BNH, (*d*) Mo@BNH, (*e*) Pd@BNH, and (*f*) Cd@BNH heteroclusters

(PDOS) and overlap DOS (OPDOS) is valuable for visualising orbital composition analysis. PDOS function of fragment A is defined as

$$\mathrm{PDOS}_A(E) = \sum_i \Xi_{i,A} F(E - \epsilon_i), \tag{3}$$

where $\Xi_{i,A}$ is the composition of fragment A in orbital i. The OPDOS between fragment A and B is defined as

$$\mathrm{OPDOS}_{A,B}(E) = \sum_i X^i_{A,B} F(E - \epsilon_i), \tag{4}$$

where $X^i_{A,B}$ is the composition of the total cross term between fragment A and B in orbital i. In the TDOS map, each discrete vertical line corresponds to a molecular orbital (MO), and the dashed line highlights the position of HOMO. The curve is the TDOS simulated based on the distribution of MO energy levels. Regarding the adsorption behaviour of hydrogen by Cr@BN, Ni@BN, Zn@BN, Mo@BN, Pd@BN, and Cd@BN nanoclusters, TDOS has been evaluated. This factor can demonstrate the existence of important chemical interactions often on the convex side (Fig. 2).

The maximum energy of TDOS for Cr@BNH (Fig. 2, *a*) with a sharp peak of –0.4 a.u. and a maximum density of states of 20 has been shown. Moreover, the amounts of TDOS for complexes of Ni@BNH (Fig. 2, *b*)

with two sharp peaks around –0.35 and –0.45 a.u. have been observed. Zn@BNH (Fig. 2, *c*) and Cd@BNH (Fig. 2, *f*) with one sharp peak around –0.75 a.u. and maximum density TDOS of 36 (Zn@BNH) and 25 (Cd@BNH) have been indicated. Mo@BNH (Fig. 2, *d*) around –0.45 a.u. and Pd@BNH (Fig. 2, *e*) around –0.3 and –0.5 a.u. have shown some fluctuations for TDOS. Therefore, the order ability of hydrogen adsorption by doping atoms of Cr, Ni, Zn, Mo, Pd, Cd on BN based on the TDOS might be shifted as Zn@BN ≈ Cd@BN > Pd@BN > Ni@BN ≈ Mo@BN > Cr@BN.

Fragment 1 has been defined for N(9), *X*(13) (*X* = Cr, Ni, Zn, Mo, Pd, Cd) of Cr@BN, Ni@ BN, Zn@ BN, Mo@ BN, Pd@BN, and Cd@BN heteroclusters and H16, H17 for hydrogenated complexes of Cr@BNH, Ni@BNH, Zn@ BNH, Mo@ BNH, Pd@BNH, and Cd@BNH through OPDOS graphs. Moreover, the fluctuation of B(1), N(2), N(3), B(4), B(5), B(6), N(7), N(8), N(14)N (15) for *X*-doped BN and BNH heterostructures of Fragment 2 and Fragment 3 through OPDOS graphs have been observed (Figs. 2, *a*–*f*).

3.2. Insight into Nuclear Quadrupole Resonance (NQR)

The NQR method relates to the multipole expansion in Cartesian co-ordinates as [49, 50]

$$V(\boldsymbol{r}) = V(\mathbf{0}) + \left.\frac{\partial V}{\partial \boldsymbol{x}_i}\right|_0 \boldsymbol{x}_i + \frac{1}{2}\left.\frac{\partial^2 V}{\partial \boldsymbol{x}_i \boldsymbol{x}_j}\right|_0 \boldsymbol{x}_i \boldsymbol{x}_j + \ldots. \tag{5}$$

After that, a simplification of Eq. (5), there are only the second derivatives related to the identical variable for the potential energy [49–52]:

$$U = -\frac{1}{2}\int_D d^3 r \rho_r \left.\frac{\partial^2 V}{\partial \boldsymbol{x}_i^2}\right|_0 \boldsymbol{x}_i^2 = -\frac{1}{2}\int_D d^3 r \rho_r \left.\frac{\partial \boldsymbol{E}_i}{\partial \boldsymbol{x}_i}\right|_0 \boldsymbol{x}_i^2 = -\frac{1}{2}\left.\frac{\partial \boldsymbol{E}_i}{\partial \boldsymbol{x}_i}\right|_0 \int_D d^3 r \rho(r)\, \boldsymbol{x}_i^2. \tag{6}$$

There are two parameters, which must be gotten from NQR experiments: the quadrupole coupling constant, χ, and the asymmetry parameter of the EFG tensor, η:

$$\chi = e^2 \boldsymbol{Q} q_{zz}/h, \tag{7}$$

$$\eta = q_{xx} - q_{yy}/q_{zz}. \tag{8}$$

The electric potential over the electric charge has been evaluated for Cr@BNH, Ni@BNH, Zn@BNH, Mo@BNH, Pd@BNH, and Cd@BNH complexes (Tables 1 and 2).

The amounts indicate that with the increase in the negative charge of different atoms, the electric potential resulting from NQR calculations increases. Moreover, the doping atoms of Cr(13), Ni(13), Zn(13), Mo(13), Pd(13), Cd(13) on the BN have shown the most potential for accepting the electron from the electron donor of H(16) and H(17) in H_2 adsorbed on the BN (Tables 1 and 2 and Fig. 3).

Table1. **The electric potential E_p and Bader charge Q through NQR calculation for Cr@BNH, Ni@BNH, and Zn@BNH heteroclusters**

Cr@BNH			Ni@BNH			Zn@BNH		
Element	Q, C	E_p, a.u.	Element	Q, C	E_p, a.u.	Element	Q, C	E_p, a.u.
B(1)	0.131	−11.287	B(1)	0.150	−11.291	B(1)	0.115	−11.296
N(2)	−0.061	−18.292	N(2)	−0.060	−18.285	N(2)	−0.039	−18.295
N(3)	−0.115	−18.301	N(3)	−0.064	−18.263	N(3)	−0.076	−18.264
B(4)	0.130	−11.287	B(4)	0.150	−11.291	B(4)	0.115	−11.296
B(5)	0.135	−11.288	B(5)	0.147	−11.291	B(5)	0.111	−11.296
B(6)	0.133	−11.288	B(6)	0.147	−11.291	B(6)	0.111	−11.296
N(7)	−0.043	−18.274	N(7)	−0.082	−18.289	N(7)	−0.061	−18.285
N(8)	−0.114	−18.301	N(8)	−0.063	−18.261	N(8)	−0.076	−18.263
N(9)	−0.190	−18.278	N(9)	−0.133	−18.272	N(9)	−0.261	−18.293
N(10)	−0.192	−18.278	N(10)	−0.134	−18.272	N(10)	−0.262	−18.293
N(11)	−0.193	−18.278	N(11)	−0.134	−18.272	N(11)	−0.261	−18.293
N(12)	−0.189	−18.278	N(12)	−0.134	−18.272	N(12)	−0.261	−18.293
Cr(13)	0.609	−14.441	Ni(13)	0.266	−23.549	Zn(13)	0.862	−16.158
N(14)	−0.042	−18.274	N(14)	−0.082	−18.289	N(14)	−0.061	−18.285
N(15)	−0.061	−18.292	N(15)	−0.060	−18.285	N(15)	−0.039	−18.295
H(16)	−0.155	−1.000	H(16)	−0.072	−1.0369	H(16)	−0.134	−0.9939
H(17)	0.220	−0.975	H(17)	0.162	−1.012	H(17)	0.218	−0.9542

Table 2. **The same as in the previous table, but for Mo@BNH, Pd@BNH,and Cd@BNH heteroclusters**

Mo@BNH			Pd@BNH			Cd@BNH		
Element	Q, C	E_p, a.u.	Element	Q, C	E_p, a.u.	Element	Q, C	E_p, a.u.
B(1)	0.136	−11.303	B(1)	0.141	−11.292	B(1)	0.119	−11.299
N(2)	−0.092	−18.313	N(2)	−0.069	−18.288	N(2)	−0.050	−18.300
N(3)	−0.051	−18.304	N(3)	−0.071	−18.272	N(3)	−0.077	−18.267
B(4)	0.136	−11.303	B(4)	0.141	−11.292	B(4)	0.120	−11.299
B(5)	0.137	−11.303	B(5)	0.139	−11.292	B(5)	0.117	−11.299
B(6)	0.137	−11.303	B(6)	0.139	−11.292	B(6)	0.117	−11.299
N(7)	−0.107	−18.318	N(7)	−0.078	−18.292	N(7)	−0.064	−18.293
N(8)	−0.050	−18.302	N(8)	−0.068	−18.270	N(8)	−0.077	−18.266
N(9)	−0.276	−18.298	N(9)	−0.135	−18.272	N(9)	−0.195	−18.301
N(10)	−0.285	−18.297	N(10)	−0.135	−18.271	N(10)	−0.196	−18.301
N(11)	−0.284	−18.297	N(11)	−0.135	−18.271	N(11)	−0.196	−18.301
N(12)	−0.277	−18.298	N(12)	−0.135	−18.272	N(12)	−0.195	−18.301
Mo(13)	1.043	−10.595	Pd(13)	0.326	−16.166	Cd(13)	0.609	−10.045
N(14)	−0.107	−18.318	N(14)	−0.078	−18.292	N(14)	−0.064	−18.293
N(15)	−0.092	−18.313	N(15)	−0.069	−18.288	N(15)	−0.050	−18.300
H(16)	−0.269	−0.9544	H(16)	−0.077	−1.026	H(16)	−0.104	−0.990
H(17)	0.304	−0.9155	H(17)	0.166	−1.013	H(17)	0.189	−0.961

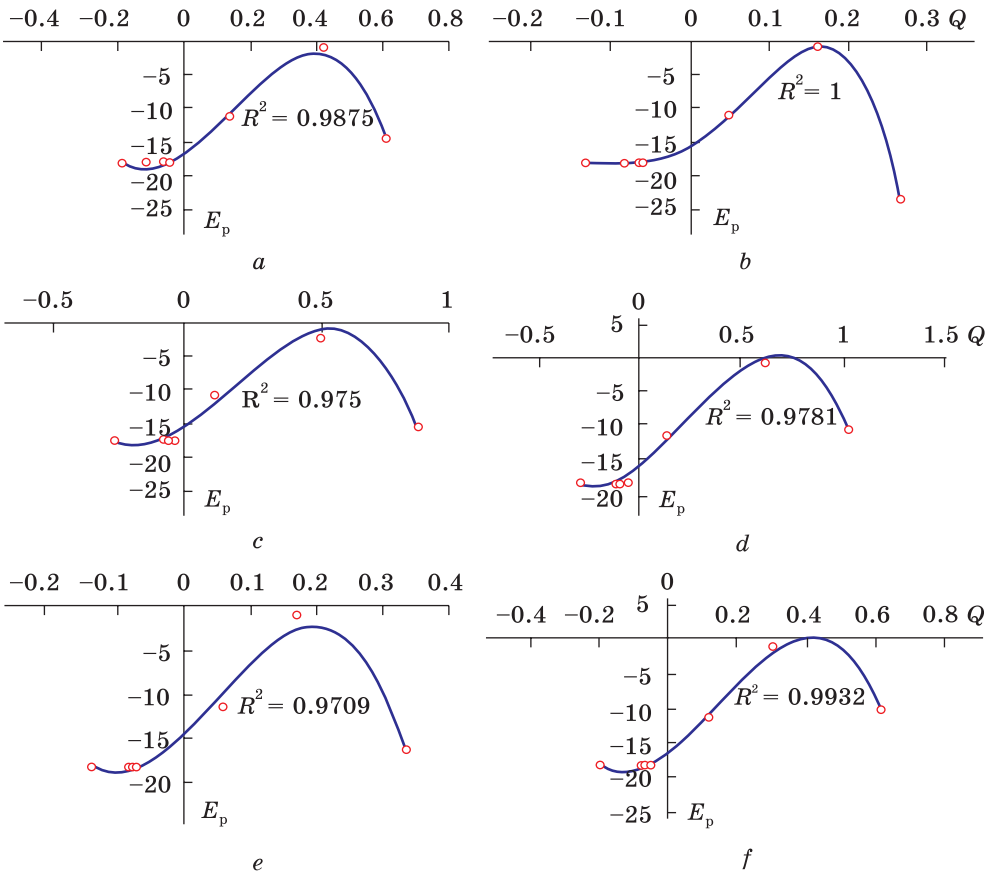

Fig. 3. Electric potential (a.u.) versus Bader charge (C) through NQR calculation for (*a*) Cr@ BNH, (*b*) Ni@BNH, (*c*) Zn@BNH, (*d*) Mo@BNH, (*e*) Pd@BNH, and (*f*) Cd@BNH heteroclusters

The curve of [Cr, Ni, Zn, Mo, Pd, Cd]@BN is waved by these H_2 molecules. The fluctuated peaks for electric potential have been shown around H_2 trapping on the [Cr, Ni, Zn, Mo, Pd, Cd]@BN which demonstrates the electron-accepting specifications of hydrogen versus the chromium, nickel, zinc, molybdenum, palladium, and cadmium doped on the BNNc (Fig. 3, *a*–*f*).

Besides, it can be considered that nickel (Fig. 3, *b*) and cadmium (Fig. 3, *f*), as the first and second row of transition metals in the periodic table, respectively, in the functionalized BNNc might have more impressive sensitivity for accepting the electrons from H atoms in the process of the adsorption mechanism. However, molybdenum-doped on BNNc (adsorbent) has shown the lowest fluctuation (R^2 = 0.9781) between Bader charge versus electric potential extracted from NQR parameters and the lowest negative atomic charge including 1.0432 coulomb on the Mo@BN complex which has the lowest tendency for H_2 adsorption after Zn with 0.8620 cou-

lomb on the Zn@BN complex and Cr or Cd with 0.6093 coulomb on the Cr@BN or Cd@BN complexes (Tables 1 and 2). Nickel and palladium with atomic charges of 0.2658 and 0.3266 coulomb on the complexes of Ni–BNNc and Pd–BNNc, respectively, have shown much more tendency for H_2 adsorption than other complexes.

3.3. NMR Spectra

Based on the resulting amounts, nuclear magnetic resonance (NMR) spectra of [Cr, Ni, Zn, Mo, Pd, Cd]@BN complexes as potential molecules for H_2 storage can unravel the efficiency of [Cr, Ni, Zn, Mo, Pd, Cd]@BN for saving clean energy.

From the DFT calculations, the chemical shielding (CS) tensors in the principal axes system have been obtained to estimate the isotropic chemical-shielding (CSI) and anisotropic chemical-shielding (CSA) [53]:

$$\sigma_{iso} = (\sigma_{11} + \sigma_{22} + \sigma_{33})/3, \quad (9)$$

$$\sigma_{aniso} = \sigma_{33} - (\sigma_{22} + \sigma_{11})/2. \quad (10)$$

The NMR data of isotropic (σ_{iso}) and anisotropic shielding tensors (σ_{aniso}) of hydrogen molecules trapped in the (Cr, Ni, Zn, Mo, Pd, Cd)@BN towards formation of Cr@BNH, Ni@BNH, Zn@BNH, Mo@BNH, Pd@BNH, and Cd@BNH complexes have been computed (Tables 3 and 4).

Table 3. **NMR parameters for Cr@BNH, Ni@BNH, and Zn@BNH heteroclusters**

Cr@BNH			Ni@BNH			Zn@BNH		
Element	σ_{iso}, ppm	σ_{aniso}, ppm	Element	σ_{iso}, ppm	σ_{aniso}, ppm	Element	σ_{iso}, ppm	σ_{aniso}, ppm
B(1)	70.258	58.794	B(1)	300.633	683.375	B(1)	68.938	212.509
N(2)	1365.305	2043.337	N(2)	7410.914	44923.490	N(2)	7461.992	8805.659
N(3)	619.512	1587.386	N(3)	8440.899	22135.347	N(3)	5626.334	19678.419
B(4)	70.111	60.276	B(4)	300.313	682.332	B(4)	68.592	214.133
B(5)	68.858	57.353	B(5)	300.370	684.009	B(5)	67.058	212.566
B(6)	68.532	59.866	B(6)	300.216	683.573	B(6)	67.397	213.379
N(7)	68.178	584.893	N(7)	3333.700	21040.918	N(7)	3095.819	14805.572
N(8)	118.722	1254.148	N(8)	8510.964	22312.556	N(8)	5726.784	19580.015
N(9)	435.373	1453.125	N(9)	1569.819	9173.706	N(9)	598.196	8738.028
N(10)	459.719	1446.933	N(10)	1588.751	9023.924	N(10)	594.407	8734.551
N(11)	440.914	1402.275	N(11)	1595.174	9119.798	N(11)	573.764	8745.053
N(12)	458.748	1487.024	N(12)	1560.476	9091.057	N(12)	572.007	8647.375
Cr(13)	15044.244	7802.678	Ni(13)	29284.054	56000.408	Zn(13)	248.778	2109.013
N(14)	61.855	594.186	N(14)	3335.625	21081.453	N(14)	3103.049	14779.110
N(15)	1348.213	2093.252	N(15)	7432.717	44860.246	N(15)	7514.916	8838.806
H(16)	61.268	101.122	H(16)	53.130	151.904	H(16)	45.217	75.754
H(17)	34.488	32.287	H(17)	0.564	48.776	H(17)	31.968	36.678

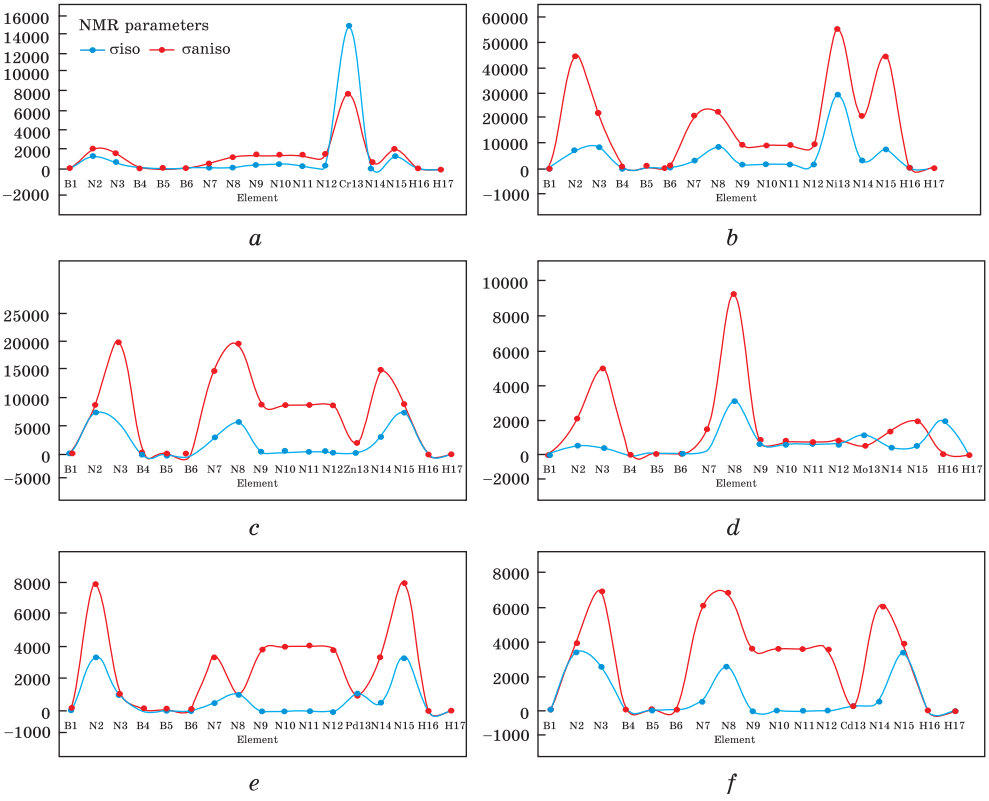

Fig. 4. The NMR spectra for (*a*) Cr@BNH, (*b*) Ni@BNH, (*c*) Zn@BNH, (*d*) Mo@BNH, (*e*) Pd@BNH, and (*f*) Cd@BNH complexes using CAM–B3LYP–D3/6–311 + G (d,p), LANL2DZ

In Tables 3 and 4, the NMR data report the notable amounts of H_2 molecules, which were adsorbed on the [Cr, Ni, Zn, Mo, Pd, Cd]@BN. The observed increase in the chemical shift anisotropy spans for H atoms adsorption on the [Cr, Ni, Zn, Mo, Pd, Cd]@BN are near N(2), N(3), N(7), N(8), N(14) and N(15).

Figure 4 illustrates the same tendency of shielding for boron and nitrogen; however, a considerable deviation exists from doping atoms of Cr(13), Ni(13), Zn(13), Mo(13), Pd(13), Cd(13) through interaction with H(16) and H(17) of H_2 molecules during adsorption on the BNNc pristine.

In Figure 4, *a*–*f*, H_2 molecules in the complexes of Cr@BNH (Fig. 4, *a*), Ni@BNH (Fig. 4, *b*), Zn@BNH (Fig.4, *c*), Mo@BNH (Fig. 4, *d*), Pd@BNH (Fig. 4, *e*), and Cd@BNH (Fig. 4, *f*) denote the fluctuation in the chemical shielding during ion trapping.

Figure 4, *a*–*f* shows the gap chemical shielding between chromium, nickel, zinc, molybdenum, palladium, and cadmium doping of [Cr, Ni, Zn, Mo, Pd, Cd]@BN complexes and hydrogen molecules. The yield of electron

accepting for doping atoms on the [Cr, Ni, Zn, Mo, Pd, Cd]@BN complexes through hydrogen molecules adsorption can be ordered as: Ni > Pd >> Cr > > Mo ≈ Zn > Cd that approves the possibility of covalent bond between chromium, nickel, zinc, molybdenum, palladium, and cadmium, and hydrogen atoms in H_2 molecules towards energy storage in battery technology.

3.4. Infrared Spectroscopy

The infrared calculations have been accomplished for the adsorption of H_2 molecules by [Cr, Ni, Zn, Mo, Pd, Cd]@BN during hydrogen sensing. So, several heteroclusters have been modelled: Cr@BNH (Fig. 5, *a*), Ni@BNH (Fig. 5, *b*), Zn@BNH (Fig. 5, *c*), Mo@BNH (Fig. 5, *d*), Pd@BNH (Fig. 5, *e*), and Cd@BNH (Fig. 5, *f*).

The chart of Fig. 5, *a* has been seen in the frequency range between 100–1100 cm^{-1} for Cr@BNH with several sharp peaks around 370.79, 506.23, 582.86, 606.67, 750.79 and 827.10 cm^{-1}. Figure 5 (*b*) shows the frequency range between 50–1200 cm^{-1} for Ni@BNH with sharp peaks around 77.24, 114.98, 244.25, 573.88, and 718.47 cm^{-1}. Figure 5, *c* shows the fluctuation of frequency between 500 and 5100 cm^{-1} for Zn@BNH with pointed peaks around 173.84, 567.81, 663.90, and 5089.68 cm^{-1}. The graph of Fig. 5, *d* has been perceived in the frequency range between

Table 4. **The same as in the previous table, but for selected atoms of Mo@BNH, Pd@BNH, and Cd@BNH heteroclusters**

Mo@BNH			Pd@BNH			Cd@BNH		
Element	σ_{iso}, ppm	σ_{aniso}, ppm	Element	σ_{iso}, ppm	σ_{aniso}, ppm	Element	σ_{iso}, ppm	σ_{aniso}, ppm
B(1)	59.534	58.917	B(1)	96.359	168.366	B(1)	66.753	105.224
N(2)	534.847	2068.889	N(2)	3381.377	7908.529	N(2)	3343.747	3860.289
N(3)	419.126	4987.964	N(3)	1028.980	1121.605	N(3)	2534.348	6807.295
B(4)	62.280	60.600	B(4)	96.346	167.966	B(4)	66.656	105.441
B(5)	61.852	84.959	B(5)	95.326	166.348	B(5)	66.343	105.650
B(6)	61.323	91.147	B(6)	95.316	166.231	B(6)	66.366	105.623
N(7)	375.182	1463.340	N(7)	571.006	3385.670	N(7)	585.266	5978.955
N(8)	3129.084	9298.234	N(8)	1062.704	1136.304	N(8)	2550.210	6802.588
N(9)	656.821	876.566	N(9)	37.254	3835.706	N(9)	35.213	3556.652
N(10)	639.759	778.044	N(10)	44.349	4015.940	N(10)	39.288	3557.941
N(11)	661.955	775.097	N(11)	42.931	4027.371	N(11)	34.056	3566.060
N(12)	643.496	844.800	N(12)	35.009	3825.071	N(12)	31.180	3532.106
Mo(13)	1131.978	514.148	Pd(13)	1115.048	1036.646	Cd(13)	243.954	307.642
N(14)	418.694	1345.758	N(14)	571.552	3384.700	N(14)	586.648	5973.052
N(15)	527.860	1989.268	N(15)	3382.212	7909.511	N(15)	3351.761	3863.718
H(16)	1989.268	62.680	H(16)	23.532	45.317	H(16)	42.978	23.694
H(17)	26.896	21.993	H(17)	21.392	7.343	H(17)	31.485	13.105

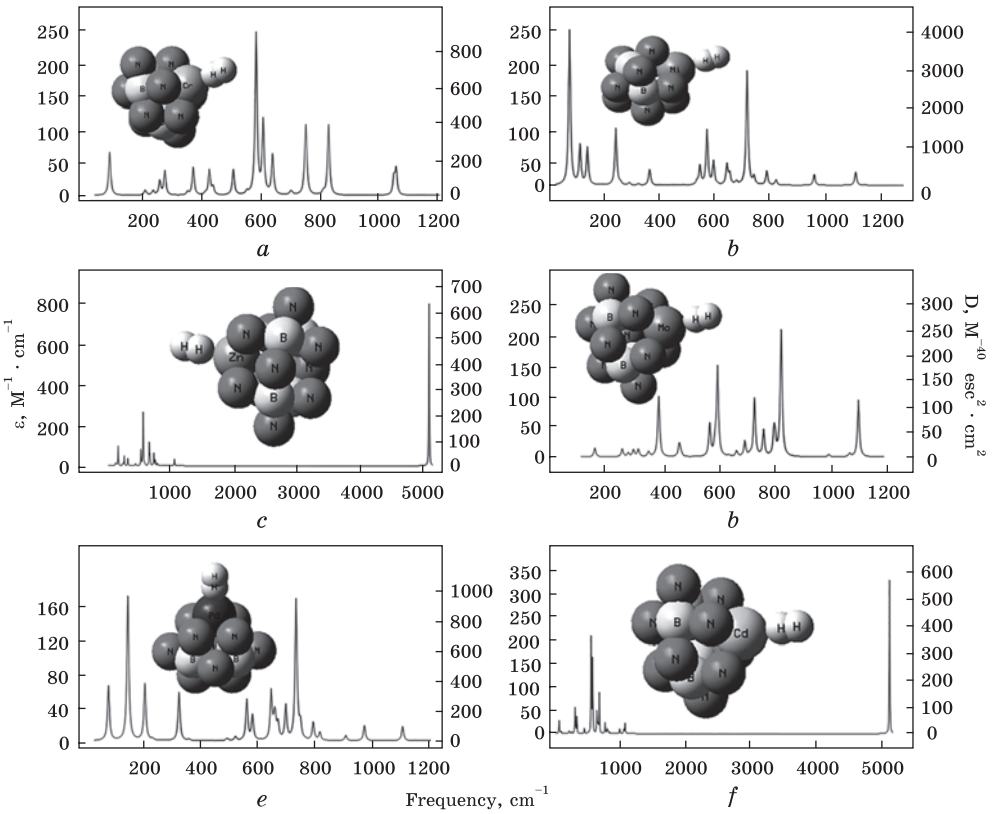

Fig. 5. IR spectra for (*a*) Cr@BNH, (*b*) Ni@BNH, (*c*) Zn@ BNH, (*d*) Mo@BNH, (*e*) Pd@ BNH, and (*f*) Cd@BNH heteroclusters

100–1200 cm^{-1} for Mo@BNH with several sharp peaks around 393.04, 604.51, 736.86, 832.58, and 1109.51 cm^{-1}. Figure 5, *e* presents the frequency range between 100 and 1200 cm^{-1} for Pd@BNH with pointed peaks around 148.81, 327.29, 563.40, and 734.87 cm^{-1}. Figure 5, *f* has remarked on the fluctuation of frequency between 100–5200 cm^{-1} for Cd@BNH with sharp peaks around 303.53, 548.81, 569.92, 674.82, and 5122.66 cm^{-1}.

The IR spectra of H_2 adsorption with [Cr, Ni, Zn, Mo, Pd, Cd]@BN have illustrated that the structure of the dominant complex correlates with the electron potency of doped Cr, Ni, Zn, Mo, Pd, Cd on the BN. The doped nanocage of Zn@BN (Figure 5c) and Cd@BN (Figure 5f) has shown the lowest fluctuations and the lowest tendency for adsorption of H_2 molecules compared to Cr@BN, Ni@BN, Mo@BN, and Pd@BN complexes, respectively (Fig. 5, *a*, *b*, *d*, *e*). Therefore, it can be found that IR spectroscopy of H_2-adsorbed Ni@BN (Fig. 5, *b*) and Pd@BN (Fig. 5, *e*) with two notable sharp peaks is now well-placed to address specific questions on the individual effect of charge carriers (hydrogen molecule-nanocage), as well as doping atoms on the overall structure.

From Table 5, through the thermodynamic specifications, it is concluded that [Cr, Ni, Zn, Mo, Pd, Cd]@BN, due to the adsorption of H_2, might be more efficient molecules for absorbing hydrogen.

The changes of Gibbs free energy versus dipole moment in Table 5 could detect the maximum efficiency of Cr, Ni, Zn, Mo, Pd, Cd atoms doping of BN pristine for H_2 molecules adsorption through ΔG_R^0 which depends on the covalent bond between H_2 molecules and (Cr, Ni, Zn, Mo, Pd, Cd)@BN.

The adsorption process of H_2 molecules on the [Cr, Ni, Zn, Mo, Pd, Cd]@BN is affirmed by the ΔG_{ads}^0 quantities:

$$\Delta G_{ads}^0 = \Delta G_{H_2\rightarrow(Cr,Ni,Zn,Mo,Pd,Cd)@BN}^0 - (\Delta G_{H_2}^0 + \Delta G_{(Cr,Ni,Zn,Mo,Pd,Cd)@BN}^0 + \Delta G_{BN}^0) \quad (11)$$

Table 5 shows the key role of doped Cr, Ni, Zn, Mo, Pd, Cd during the interaction between the adsorbate of H_2 molecules as the electron donors and the adsorbent of Cr@BN, Ni@BN, Zn@BN, Mo@BN, Pd@BN, and Cd@BN nanocages as electron acceptors.

3.5. Localised Orbital Locator Analysis

Localised orbital locator (LOL) has a similar expression compared to the electron localisation function (ELF) [54],

$$\mathrm{LOL}(\mathbf{r}) = \frac{1}{1+\tau(\mathbf{r})}, \quad \tau(\mathbf{r}) = \frac{D_0(\mathbf{r})}{\frac{1}{2}\sum_i \eta_i \left|\nabla\varphi_i(\mathbf{r})\right|^2}, \quad (12)$$

$$D_0(r) = \frac{3}{10}(6\pi^2)^{2/3}[\rho_\alpha(r)^{5/3} + \rho_\beta(r)^{5/3}]. \quad (13)$$

Table 5. **The thermodynamic characters of H_2 adsorption on the Cr@BN, Ni@BN, Zn@BN, Mo@BN, Pd@BN, and Cd@BN heteroclusters**

Compound	$\Delta E^0_{ads}\times10^{-3}$, kcal/mol	$\Delta H^0_{ads}\times10^{-3}$, kcal/mol	$\Delta G^0_{ads}\times10^{-3}$, kcal/mol	S^0_{ads}, cal/K·mol	Dipole moment, *D*
BN pristine	−420.550	−420.549	−420.579	100.650	0.2020
Cr@BN	−459.205	−459.204	−459.234	98.701	3.6785
Ni@BN	−511.241	−494.946	−511.270	99.665	1.9016
Zn@BN	−446.117	−446.116	−446.147	104.582	3.4045
Mo@BN	−447.466	−447.466	−447.495	96.556	5.9041
Pd@BN	−484.505	−484.505	−484.535	102.588	2.3467
Cd@BN	−435,064	−435.063	−435.095	106.190	3.9845
Cr@BNH	−459.923	−459.923	−459.952	99.464	4.9781
Ni@BNH	−511.963	−511.962	−511.993	103.468	2.7093
Zn@BNH	−446.838	−446.838	−446.869	104.101	4.6772
Mo@BNH	−448.183	−448.183	−448.212	96.776	7.7545
Pd@BNH	−485.222	−485.221	−485.252	102.083	3.1731
Cd@BNH	−435.779	−435.779	−435.810	105.282	5.1417

Multiwfn [47, 48] also supports the approximate version of LOL defined in Ref. [55], namely, the actual kinetic energy term in LOL is replaced by a second-order gradient expansion like ELF, which may demonstrate a broad span of bonding samples. Tsirelson's [55] version of LOL can be activated by setting ELFLOL_type to 1. For special reasons, if ELFLOL_type in settings.ini is changed from 0 to 2, another formalism will be used:

$$\mathrm{LOL}(\mathbf{r}) = \frac{1}{1 + [1 / \tau(\mathbf{r})]^2}. \tag{14}$$

If the parameter ELFLOL_cut in settings.ini is set to x, then LOL will be zero where LOL is less than x.

Adsorption of hydrogen molecules by different geometrical orientations (90°, 120°, 180°) on the nanocages of Cr@BN, Ni@BN, Zn@BN, Mo@BN, Pd@BN, Cd@BN can be defined by LOL graphs owing to exploring their delocalization/localization characterizations of electrons and chemical bonds (Fig. 6, *a*–*f*).

A vaster jointed area engaged by an isosurface map for Cr@BNH with optimized adsorption at 90° (Fig. 6, *a*), Ni@BNH with optimized adsorption at 120° (Fig. 6, *b*), Zn@BNH with optimized adsorption at 120° (Fig. 6, *c*), Mo@BNH with optimized adsorption at 90° (Figure 6d), Pd@BNH with optimized adsorption at 180° (Fig. 6, *e*), and Cd@BNH with optimized adsorption at 180° (Fig. 6, *f*) means that electron delocalization in these nanoclusters is easier than other geometrical orientations through labelling atoms of N(11), Cr(13), Ni(13), Zn(13), Mo(13), Pd(13), Cd(13) and H(16).

4. Conclusion

H_2 molecules adsorption involving the [Cr, Ni, Zn, Mo, Pd, Cd]@BN nanocages has been experimented based on electrostatic interactions between the H_2 molecules and [Cr, Ni, Zn, Mo, Pd, Cd]@BN complexes. The PDOS can evaluate a determined charge assembly between hydrogen molecules and [Cr, Ni, Zn, Mo, Pd, Cd]@BN, which indicates the competition among transition metals consisting of chromium, nickel, zinc, molybdenum, palladium, and cadmium. Based on NQR analysis, nickel and palladium with atomic charges of 0.2658 and 0.3266 C on the complexes of Ni@BN and Pd@BN, respectively, have shown a much stronger tendency for H_2 adsorption than other complexes. The electromagnetic and thermodynamic properties of [Cr, Ni, Zn, Mo, Pd, Cd]@BN complexes were computed using density functional theory. This work proposes that transition metals as ferromagnetic semiconductors can be examined through doping on the nanomaterials for enhancing the adsorption potency. The transition metal doping can be an effective way to tune the magnetic properties of BN. Although various magnetic phases in BN are being investigated recently,

the transition metal co-doping is relatively less explored for engineering magnetic properties in such promising two-dimensional nanomaterials, which motivated us to investigate transition metal co-doped BN.

Acknowledgement. In successfully completing this paper and its research, the authors are grateful to Kastamonu University.

Authors' Contributions. Conceptualisation, F.M.; methodology, F.M.; software, F.M.; validation, F.M. and M.M.; formal analysis, F.M. and M.M.; investigation, F.M. and M.M.; resources, F.M. and M.M.; data curation, F.M.; original draft preparation, F.M.; review and editing, M.M.; visualisation, F.M. and M.M.; supervision, F.M.; project administration. All authors approved the final version of the manuscript.

REFERENCES

1. D. Gonzalez-Ortiz, C. Salameh, M. Bechelany, and P. Miele, Nanostructured boron nitride-based materials: synthesis and applications, *Mater. Today Adv.,* **8**: 100107 (2020);
https://doi.org/10.1016/j.mtadv.2020.100107
2. N.S. Mishra and P. Saravanan, A review on the synergistic features of hexagonal boron nitride (white graphene) as adsorbent-photo active nanomaterial. *ChemistrySelect,* **3**, No. 28: 8023 (2018);
https://doi.org/10.1002/slct.201801524
3. Q.H. Weng, X.B. Wang, X. Wang, and Y. Bando, D. Golberg, Functionalized hexagonal boron nitride nanomaterials: emerging properties and applications. *Chem. Soc. Rev.,* **45**, No. 14: 3989 (2016);
https://doi.org/10.1039/C5CS00869G
4. A.D.O. Mucoz, A. Escobedo-Morales, E. Skakerzadeh, and E.C. Anota, Effect of homonuclear boron bonds in the adsorption of DNA nucleobases on boron nitride nanosheets, *J. Mol. Liquids,* **322**: 114951 (2021);
https://doi.org/10.1016/j.molliq.2020.114951
5. D.V. Shtansky, A.T. Matveev, E.S. Permyakova, D.V. Leybo, A.S. Konopatsky, and P.B. Sorokin, Recent Progress in Fabrication and Application of BN Nanostructures and BN-Based Nanohybrids, *Nanomaterials*, **12**: 2810 (2022);
https://doi.org/10.3390/nano12162810
6. Y. Yang, Y. Peng, M.F. Saleem, Z. Chen, and W. Sun, Hexagonal Boron Nitride on III–V Compounds: A Review of the Synthesis and Applications, *Materials*, **15**: 4396 (2022);
https://doi.org/10.3390/ma15134396
7. A. Davies, J.D. Albar, A. Summerfield, J.C. Thomas, T.S. Cheng, V.V. Korolkov, E. Stapleton, J. Wrigley, N.L. Goodey, C.J. Mellor, A.N. Khlobystov, K. Watanabe, T. Taniguchi, C. Thomas Foxon, L. Eaves, S.V. Novikov, and P.H. Beton, Lattice-Matched Epitaxial Graphene Grown on Boron Nitride, *Nano Lett.*, **18**, No. 1: 498 (2018);
https://doi.org/10.1021/acs.nanolett.7b04453
8. R.S. Bangari, V.K. Yadav, J.K. Singh, and N. Sinha, Fe_3O_4-functionalized boron nitride nanosheets as novel adsorbents for removal of arsenic(III) from contaminated water, *ACS Omega,* **5**, No. 18: 10301 (2020);
https://doi.org/10.1021/acsomega.9b04295

9. Y.H. Chao, J. Zhang, H.P. Li, P.W. Wu, X.W. Li, H.H. Chang, J. He, H.F. Wu, H.M. Li, and W.S. Zhu, Synthesis of boron nitride nanosheets with N-defects for efficient tetracycline antibiotics adsorptive removal, *Chem. Eng. J.*, **387**: 124138 (2020);
https://doi.org/10.1016/j.cej.2020.124138
10. S. Shahriari, F. Mollaamin, and M. Monajjemi, Increasing the Performance of {[(1 − x − y) $LiCo_{0.3}Cu_{0.7}$] (Al and Mg doped)] O_2}, xLi_2MnO_3, $yLiCoO_2$ Composites as Cathode Material in Lithium-Ion Battery: Synthesis and Characterization, *Micromachines*, **14**: 241 (2023);
https://doi.org/10.3390/mi14020241
11. F. Mollaamin, S. Shahriari, and M. Monajjemi, Influence of Transition Metals for Emergence of Energy Storage in Fuel Cells through Hydrogen Adsorption on the MgAl Surface, *Russ. J. Phys. Chem. B,* **18**, 398 (2024);
https://doi.org/10.1134/S199079312402026X
12. Y. Guo, R.X. Wang, P.F. Wang, L. Rao, and C. Wang, Developing a novel layered boron nitride-carbon nitride composite with high efficiency and selectivity to remove protonated dyes from water, *ACS Sustain. Chem.,* **7**, No. 6: 5727(2019);
https://doi.org/10.1021/acssuschemeng.8b05150
13. U. Cardella, L. Decker, J. Sundberg, and H. Klein, Process optimization for large-scale hydrogen liquefaction, *Int. J. Hydrogen Energy*, **42**: 12339 (2017);
https://doi.org/10.1016/j.ijhydene.2017.03.167
14. A. Hammad and I. Dincer, Analysis and assessment of an advanced hydrogen liquefaction system, *Int. J. Hydrogen Energy*, **43**: 1139 (2018);
https://doi.org/10.1016/j.ijhydene.2017.10.158
15. U. Cardella, L. Decker, and H. Klein, Economically viable large-scale hydrogen liquefaction, *IOP Conf. Ser.: Mater. Sci. Eng.*, **171**: 012013 (2017);
https://doi.org/10.1088/1757-899x/171/1/012013
16. M.A. Qyyum, Y.D. Chaniago, W. Ali, H. Saulat, and M. Lee, Membrane-Assisted Removal of Hydrogen and Nitrogen from Synthetic Natural Gas for Energy-Efficient Liquefaction, *Energies*, **13**: 5023 (2020);
https://doi.org/10.3390/en13195023
17. J.J. Picero, P.J. Ramírez, S.T. Bromley, F. Illas, F. Vices, and J.A. Rodriguez, Diversity of Adsorbed Hydrogen on the TiC(001) Surface at High Coverages, *J. Phys. Chem. C*, **122**: 28013 (2018);
https://doi.org/10.1021/acs.jpcc.8b07340
18. X. Yu, X. Zhang, H. Wang, Z. Wang, G. Feng, High-Coverage H_2 Adsorption on the Reconstructed Cu_2O(111) Surface, *J. Phys. Chem. C*, **121**: 22081 (2017);
https://doi.org/10.1021/acs.jpcc.7b06361
19. B. Chettri, P.K. Patra, S. Srivastava, Lalhriatzuala, L. Zadeng, D.P. Rai, Electronic Properties of Hydrogenated Hexagonal Boron Nitride (h-BN): DFT Study, *Senhri Journal of Multidisciplinary Studies*, **4**: 72 (2019);
https://doi.org/10.36110/sjms.2019.04.02.008
20. E. Rivard, M. Trudeau, and K. Zaghib, Hydrogen Storage for Mobility: A Review, *Materials*, **12**: 1973 (2019);
https://doi.org/10.3390/ma12121973
21. Y. Arshad, M. Asghar, M. Yar, T. Bibi, and K. Ayub, Transition Metal Doped Boron Nitride Nanocages as High Performance Nonlinear Optical Materials: A DFT Study, *J. Inorg. Organomet. Polym.*, **33**: 943 (2023);
https://doi.org/10.1007/s10904-023-02546-7
22. S. Thupsuri, C. Tabtimsai, V. Ruangpornvisuti, and B. Wanno , A study of the transition metal doped boron nitride nanosheets as promising candidates for hydrogen

and formaldehyde adsorptions, *Physica E*, **134**: 114859 (2021); https://doi.org/10.1016/j.physe.2021.114859
23. S. Chahal, T.K. Sahu, S. Kar, S. J. Ray, V. Biju, and P. Kumar, Transition Metal-Doped Boron Nitride Atomic Sheets with an Engineered Bandgap and Magnetization, *J. Phys. Chem. C*, **126**, No. 49: 21084 (2022); https://doi.org/10.1021/acs.jpcc.2c06693
24. G. Henkelman, A. Arnaldsson, and H. Jynsson, A fast and robust algorithm for Bader decomposition of charge density, *Comp. Mater. Sci.*, **36**, No.3: 354 (2006); https://doi.org/10.1016/j.commatsci.2005.04.010
25. P.E. Blöchl, Projector augmented-wave method, *Phys. Rev. B*, **50**: 17953 (1994); https://doi.org/10.1103/PhysRevB.50.17953
26. J.P. Perdew, K. Burke, and M. Ernzerhof, Generalized gradient approximation made simple, *Phys. Rev. Lett.*, **77**: 3865 (1996); https://doi.org/10.1103/PhysRevLett.77.3865
27. S. Grimme, S. Ehrlich, and L. Goerigk, Effect of the damping function in dispersion corrected density functional theory, *J. Comput. Chem.*, **32**, 1456 (2011); https://doi.org/10.3390/10.1002/jcc.21759
28. M. Arrigoni and G.K.H. Madsen, Comparing the performance of LDA and GGA functionals in predicting the T lattice thermal conductivity of III-V semiconductor materials in the zincblende structure: The cases of AlAs and Bas, *Comput. Mater. Sci.*, **156**: 354 (2019); https://doi.org/10.1016/j.commatsci.2018.10.005
29. P. Hohenberg and W. Kohn, Inhomogeneous Electron Gas, *Phys. Rev. B*, **136**: B864 (1964); https://doi.org/10.1103/PhysRev.136.B864
30. W. Kohn and L.J. Sham, Self-Consistent Equations Including Exchange and Correlation Effects, *Phys. Rev.*, **140**: A1133 (1965); https://doi.org/10.1103/PhysRev.140.A1133
31. A.D. Becke, Density-functional thermochemistry. III. The role of exact exchange, *J. Chem. Phys.*, **98**: 5648 (1993); https://doi.org/10.1063/1.464913
32. C. Lee, W. Yang, and R.G. Parr, Development of the Colle–Salvetti correlation-energy formula into a functional of the electron density, *Phys Rev B*, **37**: 785 (1988); https://doi.org/10.1103/PhysRevB.37.785
33. K. Kim and K.D. Jordan, Comparison of Density Functional and MP2 Calculations on the Water Monomer and Dimer, *J. Phys. Chem.*, **98**, No. 40: 10089 (1994); https://doi.org/10.1021/j100091a024
34. P.J. Stephens, F.J. Devlin, C.F. Chabalowski, and M.J. Frisch, Ab Initio Calculation of Vibrational Absorption and Circular Dichroism Spectra Using Density Functional Force Fields, *J. Phys. Chem.*, **98**, No. 45: 11623 (1994); https://doi.org/10.1021/j100096a001
35. P. Ballone, Modeling Potential Energy Surfaces: From First-Principle Approaches to Empirical Force Fields, *Entropy*, **16**: 322 (2014); https://doi.org/10.3390/e16010322
36. F.Mollaamin, M.Monajjemi, Adsorption ability of Ga_5N_{10} nanomaterial for removing metal ions contamination from drinking water by DFT, *Int. J. Quantum Chem.*, **124**: e27348 (2024); https://doi.org/10.1002/qua.27348
37. F. Mollaamin, Anchoring of 2D layered materials of $Ge_5Si_5O_{20}$ for (Li/Na/K)-(Rb/Cs) batteries towards Eco-friendly energy storage, *BMC Chemistry.*, **19**: 233 (2025); https://doi.org/10.1186/s13065-025-01593-0

38. W. Huang, Y. Yin, X. Xu, Q. Xia, and K. Luo, Mechanism Analysis and Integrated Optimization for Reducing Low-Speed Starting Noise in Electric Vehicles, *World Electr. Veh. J.*, **17**: 63 (2026); https://doi.org/10.3390/wevj17020063
39. M.J. Frisch, G.W. Trucks, H.B. Schlegel, G.E. Scuseria, M.A. Robb et al. *Gaussian 16, Revision C.01* (Gaussian, Inc., Wallingford CT: 2016).
40. R. Dennington, T.A. Keith, and J.M. Millam, *GaussView, Version 6.06.16* (Semichem Inc., Shawnee Mission, KS: 2016).
41. F.Mollaamin and M.Monajjemi, Graphene-based resistant sensor decorated with Mn, Co, Cu for nitric oxide detection: Langmuir adsorption & DFT method, *Sensor Review*, **43**, No. 4: 266 (2023); https://doi.org/10.1108/SR-03-2023-0040
42. F.Mollaamin and M.Monajjemi, Electric and Magnetic Evaluation of Aluminum–Magnesium Nanoalloy Decorated with Germanium Through Heterocyclic Carbenes Adsorption: A Density Functional Theory Study, *Russ. J. Phys. Chem. B*, **17**: 658 (2023); https://doi.org/10.1134/S1990793123030223
43. F. Mollaamin and M. Monajjemi, Nanomaterials for Sustainable Energy in Hydrogen-Fuel Cell: Functionalization and Characterization of Carbon Nano-Semiconductors with Silicon, Germanium, Tin or Lead through Density Functional Theory Study, *Russ. J. Phys. Chem. B*, **18**: 607(2024); https://doi.org/10.1134/S1990793124020271
44. F. Mollaamin, Competitive Intracellular Hydrogen-Nanocarrier Among Aluminum, Carbon, or Silicon Implantation: a Novel Technology of Eco-Friendly Energy Storage using Research Density Functional Theory, *Russ. J. Phys. Chem. B*, **18**: 805 (2024); https://doi.org/10.1134/S1990793124700131
45. F. Mollaamin, M. Monajjemi, In Situ Ti-Embedded SiC as Chemiresistive Nanosensor for Safety Monitoring of CO, CO_2, NO, NO_2: Molecular Modelling by Conceptual Density Functional Theory, *Russ. J. Phys. Chem. B*, **18**, 49 (2024); https://doi.org/10.1134/S1990793124010159
46. F. Mollaamin, Alkali Metals Doped on Tin-Silicon and Germanium-Silicon Oxides for Energy Storage in Hybrid Biofuel Cells: A First-Principles Study, *Russ. J. Phys. Chem. B,* **19**, No. 3: 720 (2025); https://doi.org/10.1134/S1990793125700393
47. T. Lu and F. Chen, Multiwfn: A multifunctional wavefunction analyzer, *J. Comput. Chem.*, **33**: 580 (2012); https://doi.org/10.1002/jcc.22885
48. T. Lu, A comprehensive electron wavefunction analysis toolbox for chemists, Multiwfn, *J. Chem. Phys.*, **161**: 082503 (2024); https://doi.org/10.1063/5.0216272
49. Z. Trontelj, J. Pirnat, V. Jazbinšek, J. Lužnik, S. Srčič, Z. Lavrič, S. Beguš, T. Apih, V. Žagar, and J. Seliger, Nuclear Quadrupole Resonance (NQR)—A Useful Spectroscopic Tool in Pharmacy for the Study of Polymorphism, *Crystals*, **10**: 450 (2020); https://doi.org/10.3390/cryst10060450
50. R. Sciotto, I.A. Ruiz Alvarado, and W.G. Schmidt, Substrate Doping and Defect Influence on P-Rich InP(001):H Surface Properties, *Surfaces*, **7**: 79 (2024); https://doi.org/10.3390/surfaces7010006
51. J. Luo, C. Wang, Z. Wang, Q. Guo, J. Yang, R. Rui Zhou, K. Matano, T. Oguchi, and Z. Ren, NMR and NQR studies on transition-metal arsenide superconductors $LaRu_2As_2$, $KCa_2Fe_4As_4F_2$, and $A_2Cr_3As_3$, *Chinese Phys. B*, **29**: 067402 (2020); https://doi.org/10.1088/1674-1056/ab892d
52. A. Samila, O. Hotra, O. Moisiuk, M. Khobzei, and T. Kazemirskiy, Modified Transceiver Antenna for NQR Detection of Explosive Objects in Demining Condi-

tions, *Energies*, **15**: 7348 (2022);
https://doi.org/10.3390/en15197348
53. U. Sohail, F. Ullah, N.H. Binti Zainal Arfan, M.H.S. Abdul Hamid, T. Mahmood, N.S. Sheikh, and K. Ayub, Transition Metal Sensing with Nitrogenated Holey Graphene: A First-Principles Investigation, *Molecules*, **28**: 4060 (2023);
https://doi.org/10.3390/molecules28104060
54. H.L Schmider and A.D. Becke, Chemical content of kinetic energy density, *Journal of Molecular Structure: THEOCHEM.*, **527**, Nos. 1–3: 51 (2000).
https://doi.org/10.1016/S0166-1280(00)00477-255
55. V. Tsirelson and A. Stash, Analyzing experimental electron density with the localized-orbital locator, *Acta Cryst. B*, **58**: 780 (2002);
https://doi.org/10.1107/S0108768102012338

Received / Final version
30.01.2026 / 05.06.2026

Ф. Моллаамін, М. Монайджемі
Університет Кастамону, 37150 Кастамону, Туреччина

НАНОІНКАПСУЛЯЦІЯ ПЕРЕХІДНИХ МЕТАЛІВ ГІБРИДНИМ МАТЕРІАЛОМ НА ОСНОВІ НІТРИДУ БОРУ: МАЙБУТНІ ТЕНДЕНЦІЇ АДСОРБЦІЇ ВОДНЮ ДЛЯ НАКОПИЧЕННЯ ЕНЕРГІЇ

Досліджено збільшення накопичення водню шляхом легування Cr, Ni, Zn, Mo, Pd, Cd на нанокомірки нітриду Бору (BN). На основі аналізу ядерного квадрупольного резонансу Ni та Pd з атомними зарядами у 0,2658 і 0,3266 Кл на комплексах Ni@BN і Pd@BN відповідно продемонстровано набагато більшу схильність до адсорбції H_2, ніж іншими комплексами. Результати спектроскопії ядерного магнітного резонансу показали, що ефективність приймання електронів для імплантації атомів на [Cr, Ni, Zn, Mo, Pd, Cd]@BN шляхом адсорбції H_2 можна впорядкувати так: Ni > Pd >> Cr > Mo ≈ Zn > Cd. Щодо термодинамічних властивостей, то для Гідрогенових вузлів у молекулах H_2 щільності гетерокластерів декорованих елементів Cr, Ni, Zn, Mo, Pd, Cd можна представити такими комплексами: Ni@BN > > Pd@BN >> Cr@BN > Mo@BN ≈ Zn@BN > Cd@BN. Окрім того, адсорбцію водню на гетерокластері BN, легованому перехідними металами, було оцінено за допомогою аналізу повної густини станів, парціальної густини станів, парціальної густини станів з перекриттям локалізованого орбітального локатора. Зроблено висновок, що імплантований перехідним металом BN може бути використаний для розроблення нових матеріалів для адсорбції та сенсорів H_2.

Ключові слова: зберігання водню, нанокомірка нітриду Бору, легування, теорія функціонала густини